Snowfall Measurements at Wind-Exposed and Sheltered Sites in the Rocky Mountains of Southeastern Wyoming

SAMUEL A. MARLOW,[a] JOHN M. FRANK,[b] MATTHEW BURKHART,[a] BUJIDMAA BORKHUU,[a] SHELBY E. FULLER,[a] AND JEFFERSON R. SNIDER[a]

[a] *University of Wyoming, Laramie, Wyoming*
[b] *Forest Service Rocky Mountain Research Station, Fort Collins, Colorado*

(Manuscript received 9 July 2022, in final form 27 October 2023, accepted 28 November 2023)

ABSTRACT: Snowfall is an important driver of physical and biological processes in alpine systems. Previous work has shown that surface deposition of snow can vary for reasons not directly related to precipitation processes and that this variance has consequence for water budgets in snow-dominated terrestrial systems. In this work, measurements were made over several winter seasons in a forest–meadow ecotone in the Rocky Mountains of southeastern Wyoming. Two groups of measurements—both with wind-exposed and sheltered precipitation gauges—were analyzed. Reasonable agreement between snow deposition from a Hotplate gauge (exposed) and snow deposition from a SNOTEL pillow gauge (sheltered) is reported. The other result is that snow deposition is enhanced at an exposed gauge that was deployed on the leeward side of a forest–meadow edge. The enhancement is approximately a factor of 2 and varies with wind direction and speed and with upwind forest coverage. The enhancement is greater than was documented in an earlier investigation of Rocky Mountain snow deposition; however, in that study measurements were conducted above tree line.

KEYWORDS: Snowfall; Gauges; In situ atmospheric observations; Instrumentation/sensors; Surface observations; Atmosphere–land interaction

1. Introduction

Devices available for measuring precipitation include catching and noncatching precipitation gauges (Cauteruccio et al. 2021), ground-based radar (Wilson and Brandes 1979; Harrison et al. 2000; Wolfe and Snider 2012), and airborne/spaceborne radars (Matrosov 2007; Pokharel and Vali 2011; Skofronick-Jackson et al. 2017). Attainment of better understanding of the water cycle requires that the precision of these methods be investigated and that their reports of precipitation be compared.

Precipitation measurements are associated with errors, both systematic and random, and the magnitudes of these errors are substantial in measurements of snowfall acquired with catching-type gauges[1] (Goodison 1978; Rasmussen et al. 2012; Gultepe et al. 2017). Systematic error results when snow blocks a gauge opening (Goodison et al. 1998). Snowfall missed due to gauge blockage can be registered later in time, if the blockage warms, melts, and flows into the gauge's collection container, or the blockage can persist as a systematic error if wind or wind-driven sublimation remove the blockage from the gauge opening. In either case, the occurrence of blockage propagates error to assessments of snowfall (Martinaitis et al. 2015). This problem is mitigated when an electric heater is used to melt snow as it collects on a gauge opening; however, heaters increase mass loss due to sublimation and evaporation (Metcalfe and Goodison 1992; Savina et al. 2012). Registration at a later time also occurs when snow is deposited on the inner throat of a gauge (Groisman and Legates 1994; Goodison et al. 1998).

Another type of systematic error (bias) occurs when snow particles are carried over a gauge by wind (Nešpor and Servuk 1999). The snow particle catch efficiency, that is, the fraction of the actual amount measured by a gauge, is dependent on wind speed, gauge geometry, and snow particle density (Thériault et al. 2012). Several types of wind shields, most commonly the Alter shield (Alter 1937), are used to decelerate snow particles as they are wind transported toward a gauge opening. Even with these remedies, snowfall measurements associated with moderate or larger wind speeds can still be negatively biased (Nitu and Wong 2010; Thériault et al. 2012). Undercatch can also result from tilting of a gauge, induced by either wind or gauge heating/cooling (Goodison et al. 1998; Rasmussen et al. 2018), and from deployment of a weighing gauge that is not leveled (Rinehart 1983; Sieck et al. 2007).

In contrast with the previously discussed negative biases, positive bias results when fallen snow is resuspended from the surface and collected by a gauge (Goodison et al. 1998). At present, there is no reliable way to distinguish between gauge collection of resuspended snow and collection of snow that falls from clouds, although research is focused on distinguishing these processes (Meyer et al. 2012; Kennedy et al. 2022).

The abovementioned biases can propagate significant uncertainty into measurements of snowfall rate and into measurements of time-integrated rate. Herein, the latter are referred to as amount. Unbiased rates and amounts are important in many

[1] Weighing gauges, a pillow gauge, and a Hotplate gauge are the catching-type gauges analyzed herein. Noncatching gauges (i.e., disdrometers) are not considered.

Corresponding author: Samuel Marlow, smarlow2@uwyo.edu

DOI: 10.1175/JAMC-D-22-0093.1

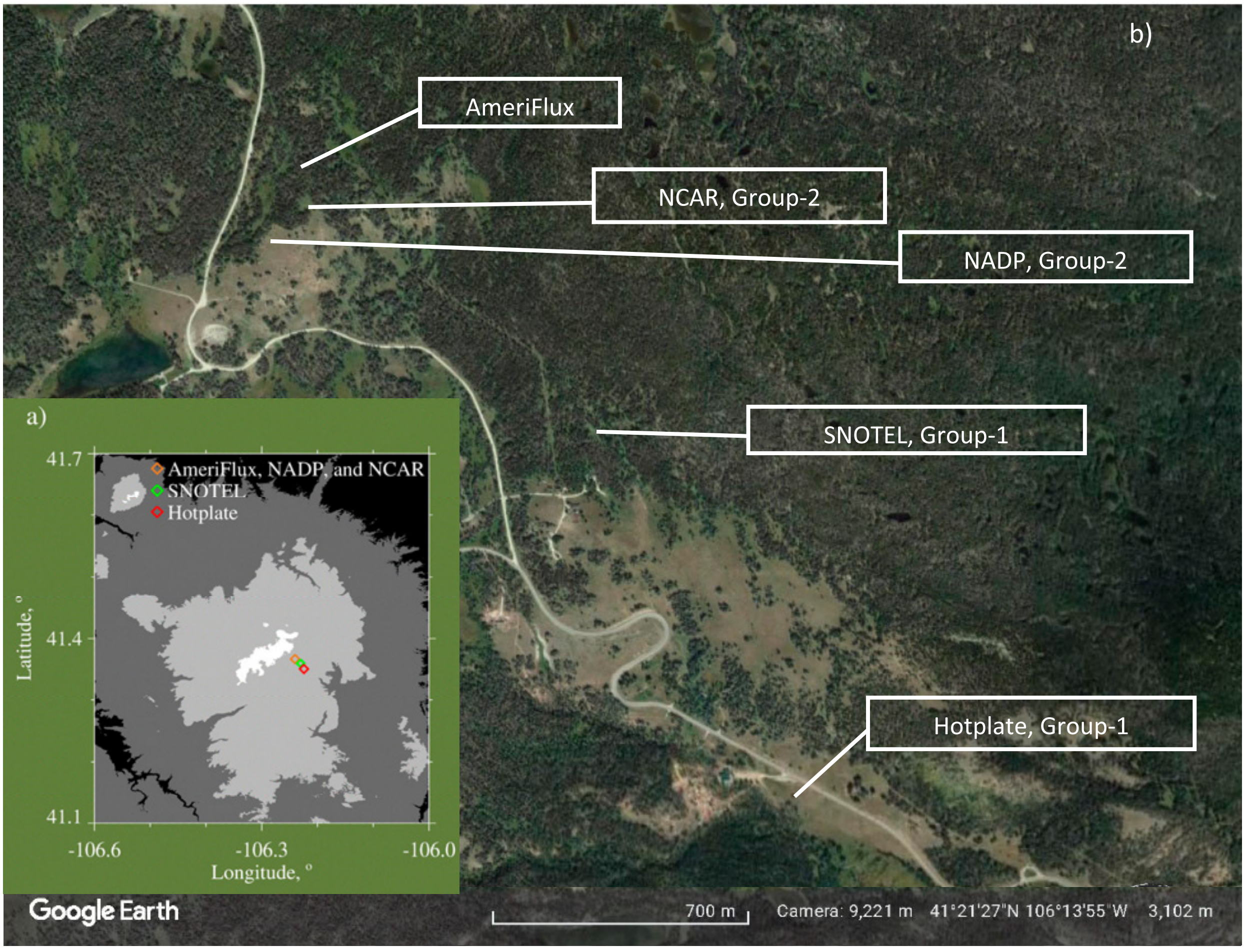

FIG. 1. (a) Map view of the Medicine Bow Mountains in southeastern Wyoming and the measurement sites. Altitude thresholds in the digital elevation map are 2300, 2800, and 3300 m. (b) Close-in satellite view of the group-1 instrument sites (SNOTEL and Hotplate), and the group-2 instrument sites (NADP and NCAR) (from Google Earth).

applications. One way that a flawed measurement can propagate error into estimates of snowfall is when gauge measurements are used to calibrate the relationship between radar reflectivity factor Z and snowfall rate S. Improving certainty in Z–S relationships is an ongoing activity involving measurements of S and coordinated radar measurements of Z (Fujiyoshi et al. 1990; Pokharel and Vali 2011; Wolfe and Snider 2012). Because surface snow amount is a key determinant of the shortwave albedo of Earth's surface (Rodell et al. 2004; Thompson and Eidhammer 2014), measurements of snowfall are also used in the initialization of weather forecasts. Hydrological and climatological models also use snowfall measurements to initialize prognostic estimates of soil moisture and runoff (Rodell et al. 2004; Kitzmiller et al. 2013; Groisman et al. 1999; Chen et al. 2002).

This research is an assessment of snowfall measurements acquired on the eastern flank of the Medicine Bow Mountains in southeastern Wyoming. The setting is a forest–meadow ecotone at approximately 3100-m elevation (Fig. 1). Measurements from both wind-exposed and sheltered precipitation gauges (both operated at ~2 m AGL), and from a wind measurement system, deployed on a tower, are analyzed. This analysis builds on a study of exposed and sheltered sites in the northern Colorado Rocky Mountains (Williams et al. 1998). The altitudes of the exposed and sheltered sites in Williams et al. (1998) were 3500 and 3750 m, and both were above the tree line. That study concluded that wind remobilization of the snowpack, and subsequent redeposition of the remobilized snow, can locally augment snow that reaches the surface from precipitating clouds. We refer to these processes as redeposition and snowfall, respectively, and refer to their combined effect as snow deposition.

The following hypothesis is tested: During snowfall events associated with a forest-to-meadow wind, snow deposition is enhanced downwind of a forest–meadow edge relative to a sheltered location. Section 2 describes the instruments. Section 3 has an elaboration of the hypothesis and describes the measurement sites and how the measurements were aggregated to test the hypothesis. Measurements are analyzed in section 4. That section also reports on data quality assurance and compares the exposed/sheltered snow deposition measurements to findings in

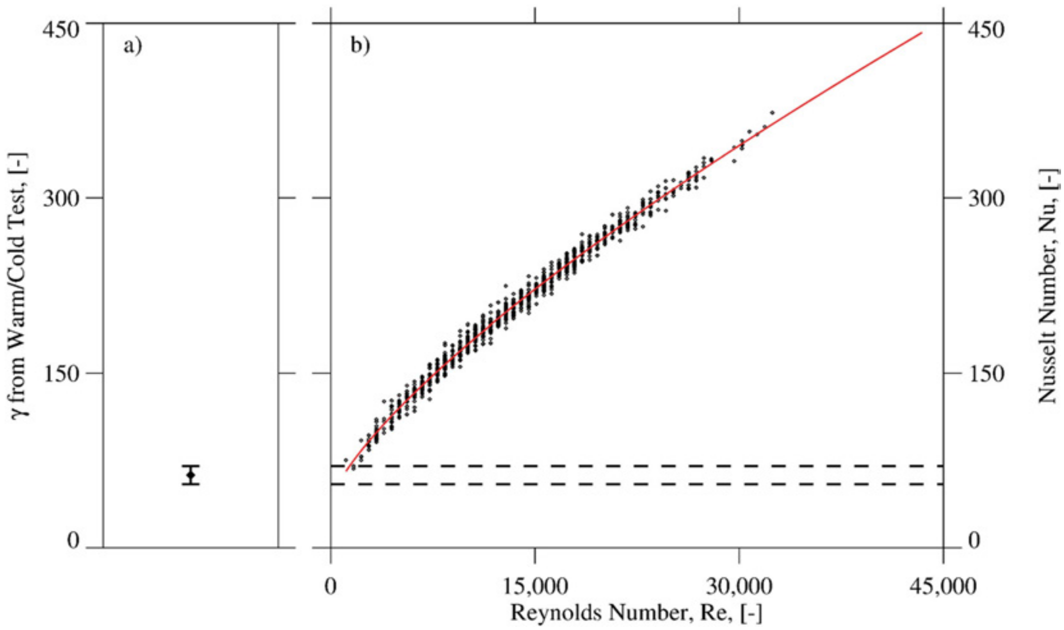

FIG. 2. (a) The upward-facing plate transport coefficient γ derived in the warm–cold test. Also plotted is the uncertainty estimate for γ (Z18). (b) The Nu–Re scatterplot and nonlinear fit to data (red line). The minimum Re plotted corresponds to wind speed = 0.2 m s^{-1}; Re values that occur with speeds smaller than this threshold were discarded. The dashed horizontal lines show the uncertainty estimate on γ from the warm–cold test.

Williams et al. (1998). Section 5 summarizes the findings of this investigation.

2. Instrumentation

Throughout this work, and consistent with meteorological convention, precipitation rate is expressed as liquid-equivalent depth per unit time and precipitation amount is expressed as liquid equivalent depth [mm; henceforth, snow water equivalent depth (SWE)].

a. Hotplate gauge

The Hotplate precipitation gauge (hereinafter Hotplate) was developed by the National Center for Atmospheric Research (NCAR) and the Desert Research Institute. The instrument is manufactured by Yankee Environmental Systems and Pond Engineering. The device's precipitation sensor is an upward-facing surface, and its wind speed sensor is a downward-facing surface. Both surfaces are apparent in Rasmussen et al. (2011) and in Zelasko et al. (2018). Going forward, these surfaces are referred to as the upward-facing plate and downward-facing plate. Both plates are controlled at approximately 70°C.

Hotplate-derived precipitation rates were obtained by applying a rate form of the upward-facing plate's first law of thermodynamics, assuming steady state (Zelasko et al. 2018, hereinafter Z18). Electric power input to the plate (electric resistive heating) and rates of sensible, latent, shortwave radiant, and longwave radiant heating/cooling are terms in the equation. The Hotplate-derived wind speed U_2 applied in the calculation is the "proprietary wind speed" discussed in Z18. Fuller et al. (2023) demonstrated that U_2 is consistent with an independently measured wind speed. Upward-facing plate calibrations are in Figs. 2a and 2b. On the y axis of Fig. 2b is a dimensionless representation of the rate of sensible cooling, and on the x axis is a dimensionless representation of wind speed. This way of describing heat transfer is adopted from Nellis and Klein (2021, their section 8.2.2). The Nusselt number Nu and Reynolds number Re pairs shown here were derived using Hotplate measurements acquired at the measurement site (Fig. 1) during a precipitation-free interval. In the Z18 algorithm, the Nu is related to Re via the red line, which is a fit of the Nu/Re pairs. The fitted relationship is $\mathrm{Nu} = 0.140\mathrm{Re}^{0.746} + 39.4$. The upward-facing plate's surface temperature ($T_h = 64$°C) is a constant both in determinations of the Nu/Re relationship and in the Z18 algorithm. The procedure developed for evaluating the upward-facing plate surface temperature and its sensible heat transport coefficient (γ = 62.4), and their uncertainties, is referred to as the warm–cold test. The T_h uncertainty was ±7°C and the γ and its uncertainty is plotted in Fig. 2a.

Hotplate-derived precipitation rate measurements were corrected for inefficient snow particle catch using a catch efficiency versus wind speed relationship, which is an extension of the relationship presented in Rasmussen et al. (2011, hereinafter R11). In R11, the particle catch efficiency is related to wind speed measured at 10 m AGL (Fig. 3a). On the x axis is the 10-m wind speed U_{10} at the site where R11 made catch efficiency measurements. In this work, Hotplate-derived wind speed values used in the catch efficiency calculation were acquired at approximately 2 m above the snowpack surface and are symbolized U_2. In Fig. 3b, U_{10} is transformed to U_2 using

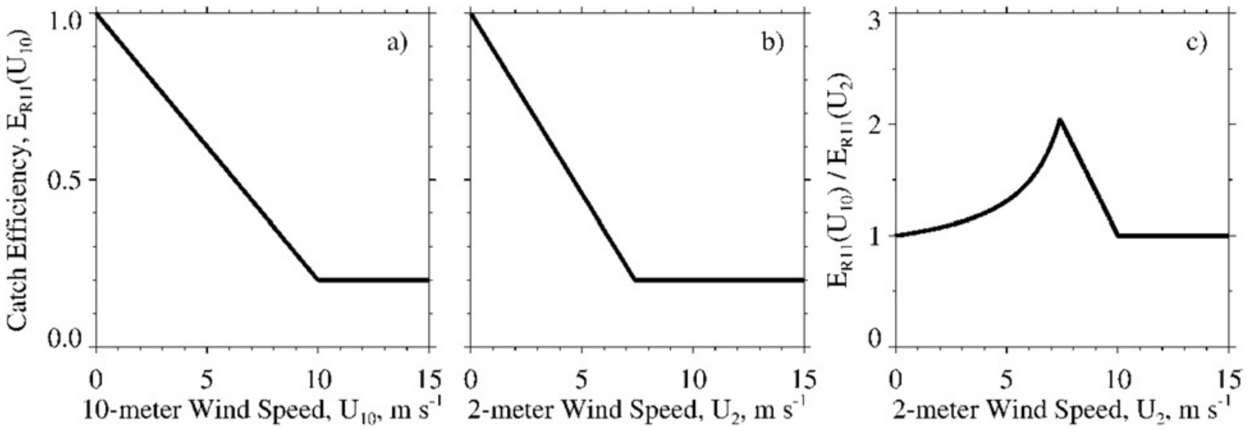

FIG. 3. (a) The Hotplate catch efficiency relationship reported in R11. Plotted on the x axis is the wind speed at 10 m AGL wind speed. (b) The modified R11 relationship applied in this work. Plotted on the x axis is the wind speed at 2 m AGL. (c) Ratio of catch efficiencies at 10 and 2 m AGL vs U_2.

the parameters $z_o = 0.01$ m and $d = 0.4$ m (Kochendorfer et al. 2018) and Eq. (6.7) from Panofsky and Dutton (1984). The Kochendorfer et al. parameters are specific to the site where R11 made their catch efficiency and U_{10} measurements. The function presented in Fig. 3b has the form $E_{R11}(U_2) = 1 - 0.108U_2$. Following R11, the catch efficiency plotted in Fig. 3b is thresholded at 0.2. The thresholding occurs at $U_2 > 7.4$ m s^{-1}. Figure 3c shows that the ratio of the two efficiencies maximizes at $U_2 = 7.4$ m s^{-1}. At $U_2 = 7.4$ m s^{-1}, precipitation rates reported herein (based on the modified relationship in Fig. 3b), are approximately a factor of 2 larger than derived using the R11 catch efficiency function. The average wind speed was 2.3 m s^{-1}, and the 75th-percentile wind speed was 3.1 m s^{-1} during 63 days with snowfall at the Hotplate site from 2015 to 2018. Wind speeds were substantially larger at 26 m on the AmeriFlux tower where these statistics were 7.4 and 9.5 m s^{-1}. This finding is evident in the graphed Hotplate and AmeriFlux time sequences referenced in the data availability statement (below).

b. SNOTEL pillow gauge

The SNOTEL pillow gauge (herein, SNOTEL) is a system that continually evaluates the mass of snowpack over a fluid-filled pillow (Serreze et al. 1999) (Fig. 4). A change of snow mass lying on the pillow is registered by a differential pressure sensor and related to SWE. SNOTEL measurements are subject to random error due to limitations of the pressure sensor and due to heating/cooling of the fluid. The magnitude of this error, during winter, is likely comparable to the smallest deviation from SWE = 0 mm during summer when no snowpack lies on the pillow. The latter is 2.4 mm (Serreze et al. 1999). Systematic error can contribute to either negative bias or positive bias, depending on circumstances. Negative bias occurs when the mass on the pillow is decreased by the formation of an ice bridge, by melting and runoff, or by wind removal of a portion of the mass. Positive bias occurs when redeposition or foliar debris contribute to the mass on the pillow. SNOTEL sites are operated by the Natural Resources Conservation Service (NRCS 2021) at approximately 800 locations, mostly in the western states of California, Oregon, Washington, Montana, Idaho, Wyoming, and Colorado.

c. AmeriFlux/R. M. Young anemometer

AmeriFlux is a network of towers and instrument packages focused on measuring CO_2, H_2O, and energy fluxes throughout the Americas. Additionally, meteorological measurements [wind, temperature T, and relative humidity (RH)] are recorded and archived. This analysis utilizes AmeriFlux 30-min-averaged horizontal wind, T, and RH recordings (AmeriFlux 2021).

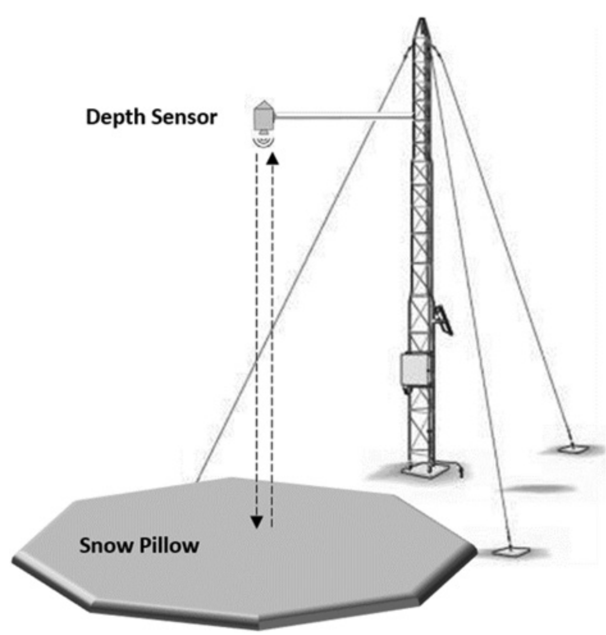

FIG. 4. Example SNOTEL site and SNOTEL pillow gauge (Colorado Avalanche Information Center 2022).

TABLE 1. Gauges and the time intervals for which data are available at the NADP and NCAR sites.

Gauge	Site	Data availability
NADP NOAH-IV	NADP	2008–present
Belfort	NADP	2011–14
NOAH1-II	NCAR	2008–14
NOAH2-II	NCAR	2008–14
NOAH3-II	NCAR	2009–14
Geonor1-T200B	NCAR	2008–14
Geonor2-T200B	NCAR	2010–14
Geonor3-T200B	NCAR	2010–14
Vaisala-VRG	NCAR	2008–10

The *T*–RH sensor and the anemometer (R. M. Young model 05103) were deployed at 23 and 26 m, respectively, on the AmeriFlux tower (Fig. 1).

d. NADP

The National Atmospheric Deposition Program (NADP 2021) is charged with quantifying the deposition of chemical constituents carried to Earth's surface by precipitation. Monitored constituents are acids, nutrients, base cations, and mercury. Each NADP site consists of two measurement systems: a sample collector and a precipitation gauge (Burns 2003). Once each week, the water within the sample collector is retrieved and sent to a laboratory where it is analyzed, and the mass concentrations of constituents are recorded. The gauge data are used to evaluate the water mass flux. The product of constituent mass concentration and water mass flux is the flux of a deposited chemical constituent. Therefore, error associated with a measurement of water mass flux propagates directly into the reporting of chemical deposition. This error is important for the estimation of chemical deposition's effects on ecological processes (Nanus et al. 2017) and can limit confidence when such measurements are used to argue for air pollutant control (Lehmann et al. 2005; Li et al. 2016). Related to these concerns, there is a strong disagreement between gauge and collector precipitation amounts at high elevation NADP sites (>3000 m) during wintertime (Borkhuu 2009). This disagreement has led to exclusion of high-elevation NADP data in nationwide assessments of chemical deposition (Lehmann et al. 2005).

Precipitation gauges operated at the NADP site (Table 1) are a "NOAH-IV" weighing gauge (ETI Instrument Systems 2020) and a Belfort weighing gauge. The former has an optical sensor that distinguishes precipitation from thermally induced gauge motion. Both of these gauges were Alter shielded.

e. NCAR gauges

Multiple precipitation gauges were operated at the NCAR site (Fig. 1) from 2008 to 2014. Gauges active at any time were combinations of three gauge types: NOAH-II, Geonor-T200B, and Vaisala-VRG (Table 1). Using the algorithm described in Rasmussen et al. (2018), sample container weight measurements acquired by the NOAH-II gauges were corrected for thermally induced gauge motion. This was also done for data acquired by the NADP NOAH-IV gauge operated at the NADP site but no significant change in that dataset was detected and so those measurements were not corrected like the NOAH-II. It is presumed this is because of the optical sensor that is a component of the NOAH-IV system (section 2d).

The NCAR gauge measurements analyzed in this study are the average of measurements available from gauges operated at the NCAR site (Breed et al. 2014). Other than the correction of the NOAH-II discussed in the previous paragraph, no other correction was applied to NCAR gauge measurements. Nearly all of these gauges were Alter shielded. Wind speeds at this site were seldom greater than 2 m s^{-1} (Breed et al. 2014) and were assumed to not impact the efficiency of snow particle collection (Goodison et al. 1998). This assumption is addressed in section 4f.

3. Measurement sites and methodology

a. Measurement sites

This study compares snowfall measurements from two groups of measurement systems (Fig. 1 and Table 2). The group-1 systems are the Hotplate gauge and the SNOTEL. These were separated horizontally by 1150 m and vertically by 110 m. The Hotplate was in a meadow, approximately 10 m northeast of a forest–meadow edge (Fig. 5), and the SNOTEL was surrounded by forest out to at least 170 m in all directions (Fig. 6). The group-2 systems are the NADP NOAH-IV gauge and the NCAR gauges (Table 1). These

TABLE 2. Sensors, group assignments, sampling intervals in the recorded data, time formats in the recorded data, site altitudes, formal names of the climate-monitoring sites (SNOTEL, NADP, and AmeriFlux), and designations as wind exposed or sheltered.

Sensor	Group	Sampling interval (s)	Time format	Site alt (m)	Formal name	Designation
Hotplate gauge	1	60-s running avg recorded at 1 Hz (Z18)	UTC	3010		Exposed
SNOTEL	1	3600	UTC − 8 h	3120	Brooklyn Lake	Sheltered
NADP NOAH-IV gauge	2	900	UTC	3190	WY95	Exposed
NCAR gauges	2	See section 3c	UTC	3190		Sheltered
R. M. Young anemometer and *T*–RH sensor	1 and 2	1800	UTC − 7 h	3200 (tower-base alt)	U.S.-GLE	Not applicable (see section 2c)
Belfort gauge	2	300	UTC − 7 h	3190	WY95	Exposed

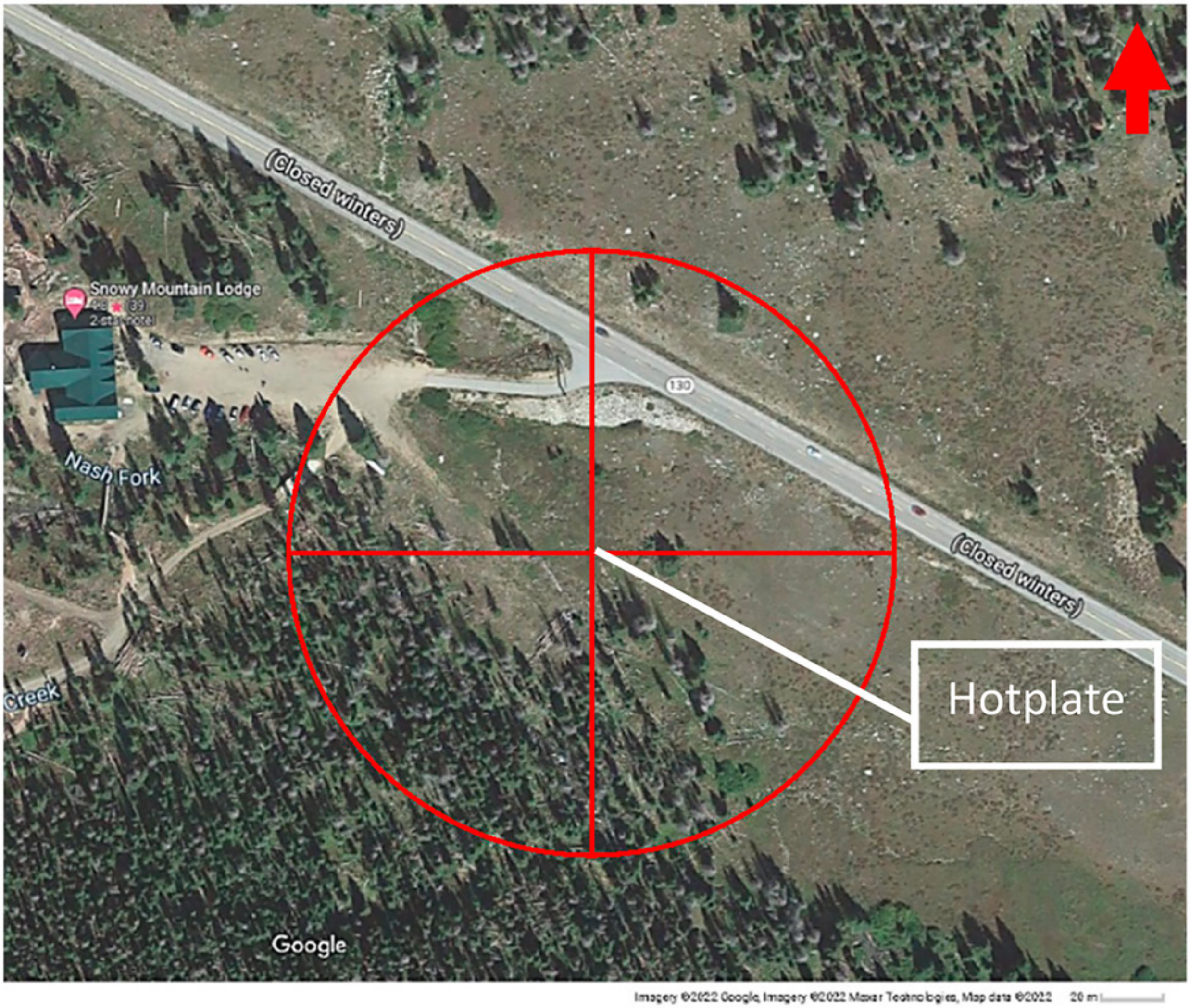

FIG. 5. Satellite view of the Hotplate site (from Google Earth). The four wind quadrants discussed in the text are indicated with red lines. North is indicated.

were separated horizontally by 140 m and vertically by less than 10 m. The NADP NOAH-IV gauge was in a meadow, approximately 20 m east of a forest–meadow edge, and the NCAR gauges were in a clearing that opens to the southeast (Fig. 7).

Table 2 has the group assignments, sampling intervals in the recorded data, time formats in the recorded data, and site altitudes for all gauge sites as well as for the two ancillary datasets that were also analyzed.

Instrumentation was removed from the NCAR and Hotplate sites in 2014 and 2017, respectively, and climate monitoring is ongoing at the other sites (SNOTEL, NADP, and AmeriFlux). Formal names of the climate-monitoring sites are provided in Table 2.

b. Snow-fence hypothesis

In this study, exposed will refer to gauges deployed on the meadow side of a forest–meadow edge. The exposed gauges were the Hotplate (Fig. 5; group 1) and the NADP NOAH-IV (Fig. 7; group 2). Sheltered gauges will refer to gauges surrounded by forest. The sheltered gauges were SNOTEL (Fig. 6; group 1) and NCAR (Fig. 7; group 2). The final column of Table 2 has these designations.

The hypothesis for data subsets with a forest-to-meadow wind is that the forest–meadow edge acts as a snow fence. Consistent with this, numerical aerodynamic simulations resolve a backward-flowing recirculation eddy that forms downwind of a forest–meadow edge. A sketch of the modeled eddy is provided in the bottom half of Fig. 14 in Cassiani et al. (2008). It is hypothesized that eddies of this type add to snow deposition at the wind-exposed sites relative to that at the sheltered sites.

The snow-fence hypothesis tested in this work has the following characteristics: 1) increased wind speed enhances the airborne transport of snow particles that detach from upwind trees, and 2) the transported particles are caught up in the recirculation eddy, located downwind of the forest–meadow edge (Cassiani et al. 2008, their Fig. 14), and redeposit there.

FIG. 6. Satellite view of the SNOTEL site (from Google Earth). North is indicated.

c. Analysis intervals

The group-1 measurements were acquired between 2015 and 2017 and the group-2 measurements were acquired between 2008 and 2014. The durations of the analysis intervals were 24 h (group 1) and 4 h (group 2). All group-1 intervals began at 0000 UTC. The start and end times of the group-2 intervals were selected by NCAR (K. Ikeda 2017, personal communication). This selection was part of a study that released ice nucleating aerosol particles and investigated the effect of the particles on snowfall (Breed et al. 2014).

Four data-rejection criteria were applied prior to analyzing the analysis intervals and associated precipitation amounts. The first rejected intervals with at least one of the paired SWE measurements $\leq$ 0 mm. The second rejected intervals warmer than -2°C on the assumption that this distinguished rainfall from snowfall. The basis for this was temperature measurements made on the AmeriFlux tower (section 2c). This is logical for the group-2 sites, which were relatively close to the AmeriFlux tower (Fig. 1) and differ in altitude from the tower's T–RH sensor by no more than 33 m (Table 2 and section 2c). The second criterion did not reject any of the group-2 intervals.

A rainfall/snowfall decision was also made for group 1. Again, this was done by applying the -2°C rainfall/snowfall threshold and temperature measurements from the AmeriFlux tower. Despite the larger altitude of the tower's T–RH sensor, when compared with the Hotplate (Table 2 and section 2c), use of the tower T measurement was necessary because the Hotplate T measurement was high biased during daytime. The Hotplate temperature bias was approximately $+3$°C with overcast skies and increased to $+7$°C in direct sun. This bias is evident in the graphed Hotplate and AmeriFlux sequences referenced in the data availability statement. The assumption applied in application of the -2°C rainfall/snowfall threshold was that the Hotplate/tower T difference was 2°C. The latter is the product of the unsaturated adiabatic lapse rate (9.8×10^{-3}°C m^{-1}) and the 210-m Hotplate-to-tower altitude difference. Support for the

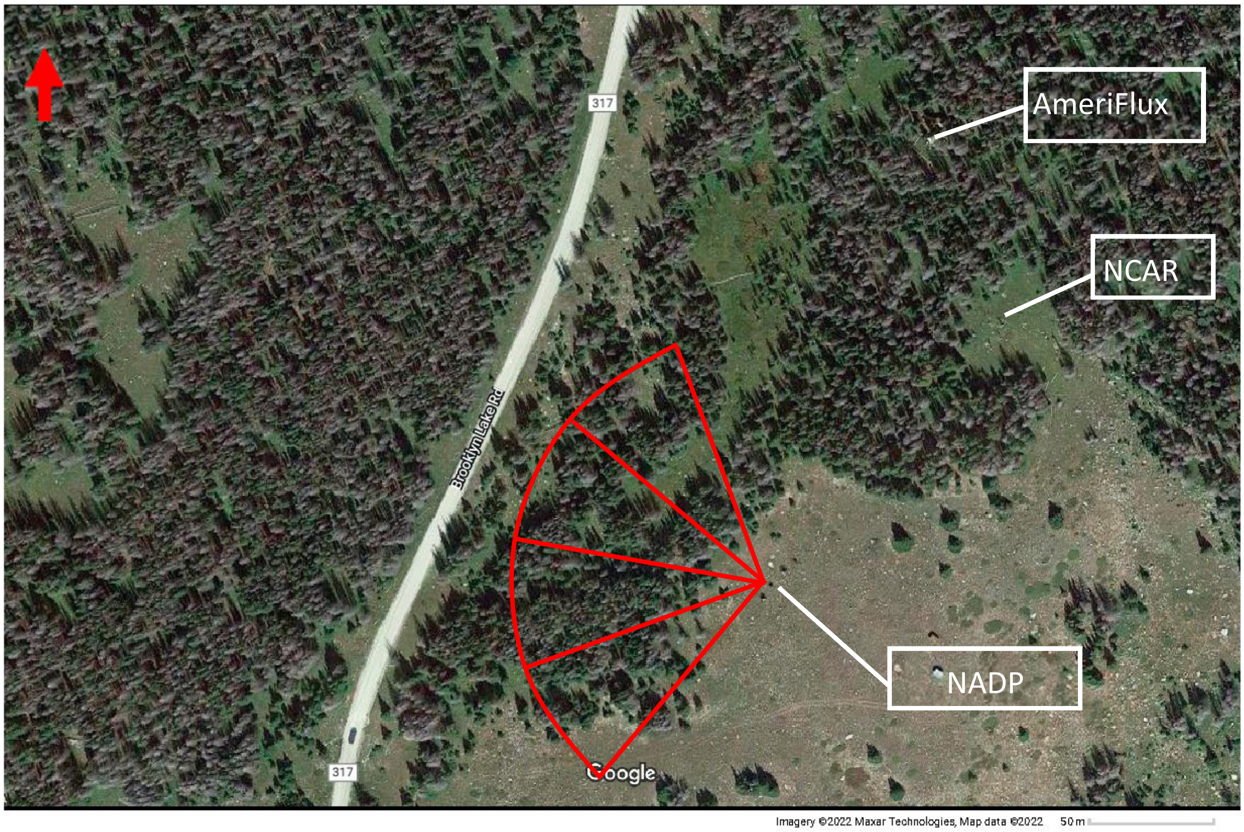

FIG. 7. Satellite view of the locations of the AmeriFlux tower, NCAR gauges, and the NADP gauges (from Google Earth). The red cones indicate the wind sectors discussed in the text: going clockwise from the lower left, the sectors are $220° \leq \theta < 250°$, $250° \leq \theta < 280°$, $280° \leq \theta < 310°$, and $310° \leq \theta < 340°$. North is indicated.

assumption comes from the fact that RH values measured on the AmeriFlux tower rarely exceeded 90% (This result is shown in the graphed AmeriFlux time sequences referenced in the data availability statement). The latter indicates that liquid cloud water was typically not present at the AmeriFlux (RH = 100% is required for this) but does not exclude the possibility that the actual Hotplate/tower T difference was smaller than 2°C due to snow particles that sublimated within air that moved downward from the tower to the Hotplate (assuming this occurred). A vertical temperature profile more stable than unsaturated adiabatic would also make the T difference smaller than 2°C. Additionally, the −2°C rainfall/snowfall threshold rests on the assumption that the temperature of a snow particle is the same as the ambient temperature. In fact, the particle temperature is approximately 0.3°C colder than the ambient temperature (Z18, their Fig. 6). If any of these unaccounted-for factors (i.e., sublimation within descending air, thermal stability, particle temperature colder than ambient temperature) were significant, then some intervals with snowfall would be interpreted as rainfall and would therefore be rejected. The second criterion (i.e., tower temperature warmer than −2°C) rejected three of the group-1 intervals.

The third criterion rejects group-2 intervals if the difference between two NADP NOAH-IV data sequences was > 1 mm. These two data sequences are now described and discussed. The NADP NOAH-IV reports a derived SWE, specific to each recording interval, and a cumulative SWE. Both are reported 4 times per hour (Table 2). Optical detection of snow particles falling into the collection container (section 2d) is necessary for the derived SWE to be reported as greater than 0 mm (ETI Instrument Systems 2020). Typically, the SWE calculated by summing the derived SWE agreed with the SWE calculated by subtracting a beginning cumulative SWE from an ending cumulative SWE, and furthermore, the agreement among these was within ±1 mm. However, a few of the group-2 intervals had the former (NADP_sum) substantially larger than the latter (NADP_sub). An example of this (Fig. 8) is

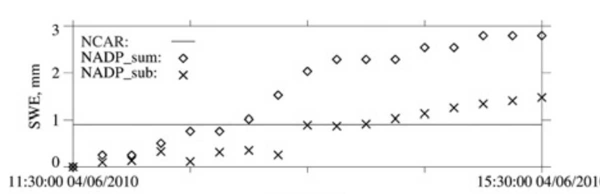

FIG. 8. One of six group-2 intervals rejected with the third criterion. Symbols indicate the two SWE sequences (NADP_sum and NADP_sub) discussed in the text.

one of six that were rejected because NADP_sum − NADP_sub was greater than 1 mm. The authors cannot explain this positive departure between the NADP_sum and NADP_sub. Henceforth, the NADP SWE values analyzed were obtained by summing values of the derived SWE.

The fourth rejection criterion is an objective statistical method that rejects measured SWE pairs that deviate strongly from the general trend of the data. This criterion was evaluated in the following three steps. First, the orthogonal displacement of a SWE pair from the one-to-one line was computed. In these calculations, larger SWE at the exposed gauge was assigned an orthogonal displacement > 0 and smaller SWE at the exposed gauge was assigned an orthogonal displacement < 0. Second, two orthogonal displacement quartiles—the first quartile (Q1; group 1 = −1.4 mm and group 2 = 0.4 mm) and the third quartile (Q3; group 1 = 1.3 mm and group 2 = 1.9 mm)—were computed. Third, pairs with orthogonal displacement outside the range [Q1 − 1.5(Q3 − Q1), Q3 + 1.5(Q3 − Q1)] were discarded as outliers (CREATBOXPLOTDATA routine from the Harris Geospatial Solutions Interactive Data Language). Group-1 analysis intervals not rejected via the first and second criteria, but rejected as outliers, are labeled as outliers in the data referenced in the data availability statement. Group-2 analysis intervals not rejected via the first, second, and third criteria, but rejected as outliers, are also labeled as outliers in the data referenced in the data availability statement.

d. *Wind direction and wind speed*

The values of wind direction and wind speed brought into the analysis were derived using horizontal wind measurements reported by the AmeriFlux anemometer (section 2c).

Interval-averaged wind direction was computed in four steps: First, the set of AmeriFlux horizontal wind vectors classified within an analysis interval were selected. Second, sets of the west-to-east and south-to-north wind components were derived. Third, the component sets were averaged over the analysis interval. Fourth, the averaged components were recomposed into an interval-averaged wind direction.

Interval-averaged wind speed was derived by averaging the AmeriFlux wind speeds that classified within an analysis interval. The authors assert that this scalar-averaged speed, as opposed to the somewhat smaller vector-averaged speed, is more relevant to the process of airborne snow particle transport.

The interval-averaged direction and interval-averaged speed were taken to characterize wind just above the tree canopy. The Hotplate wind speed measurements discussed in section 2a were applied in the Z18 algorithm but were not used to characterize the interval-averaged wind speed.

e. *Regression analysis and statistical testing*

Paired X–Y data points are compared in scatterplots that contain the regression line defined by Eq. (1):

$$Y = a + bX. \tag{1}$$

Using least squares regression, the line's intercept a, slope b, intercept standard deviation σ_a, and slope standard deviation σ_b were calculated [Young 1962, their Eqs. (15.11), (15.16), and (15.17)].

Equations (2) and (3) show how uncertainties in slope and intercept were formulated in terms of intercept and slope standard deviations and a critical value t^* derived using a t-distribution calculator (the T_CVF routine of the Interactive Data Language). Inputs to the calculator were the number of X/Y pairs (N), degrees of freedom (Df = $N - 2$), and a probability equal 0.05:

$$a \pm \sigma_a t^* \quad \text{and} \tag{2}$$

$$b \pm \sigma_b t^*. \tag{3}$$

In the scatterplots, r is the Pearson correlation coefficient, Eq. (1) is the solid line, and the dashed lines represent upper-limit and lower-limit regression threshold lines calculated as

$$Y_{\text{upper}} = (a + \sigma_a t^*) + (b + \sigma_b t^*)X \quad \text{and} \tag{4}$$

$$Y_{\text{lower}} = (a - \sigma_a t^*) + (b - \sigma_b t^*)X. \tag{5}$$

Statistical testing of the regression line's slope and intercept was also conducted. The basis for this was a probability calculated using a t-distribution calculator (the T_PDF routine from the Interactive Data Language). For the intercept, the inputs to T_PDF were Df and

$$t = \frac{|a - 0|}{\sigma_a}, \tag{6}$$

and for the slope the inputs to T_PDF were Df and

$$t = \frac{|b - 1|}{\sigma_b}. \tag{7}$$

In the statistical tests, the null hypotheses were $a = 0$ and $b = 1$, the probability that the null hypotheses were true (p value) was evaluated as 1 − the output value from T_PDF, and the critical p value was set to 0.05.

4. Results

a. *Hotplate versus SNOTEL (group 1)*

Figure 9a is a scatterplot of the group-1 analysis intervals with the wind-exposed gauge (Hotplate) on the y axis and the sheltered gauge (SNOTEL) on the x axis. The Hotplate values shown here were derived using the 2-m catch efficiency. Repeating the Hotplate SWE calculation using the 10-m catch efficiency decreases the Hotplate SWE values, and that decrease is consistent with results shown in Figs. 3a and 3b. However, because wind speed at the Hotplate was mostly < 3 m s^{-1} (section 2a) the SWE decrease is rather small. The averaged absolute difference of the two sets of Hotplate values is 0.98 mm (±0.68 mm) and the average of the ratio of the two is 0.91 (±0.05). Figures 9b and 9c show the group-1 intervals stratified by interval-averaged wind direction. The stratifications are northwest ($270° \le \theta < 360°$) (Fig. 9b) and southwest ($180° \le \theta < 270°$) (Fig. 9c). The northeast and

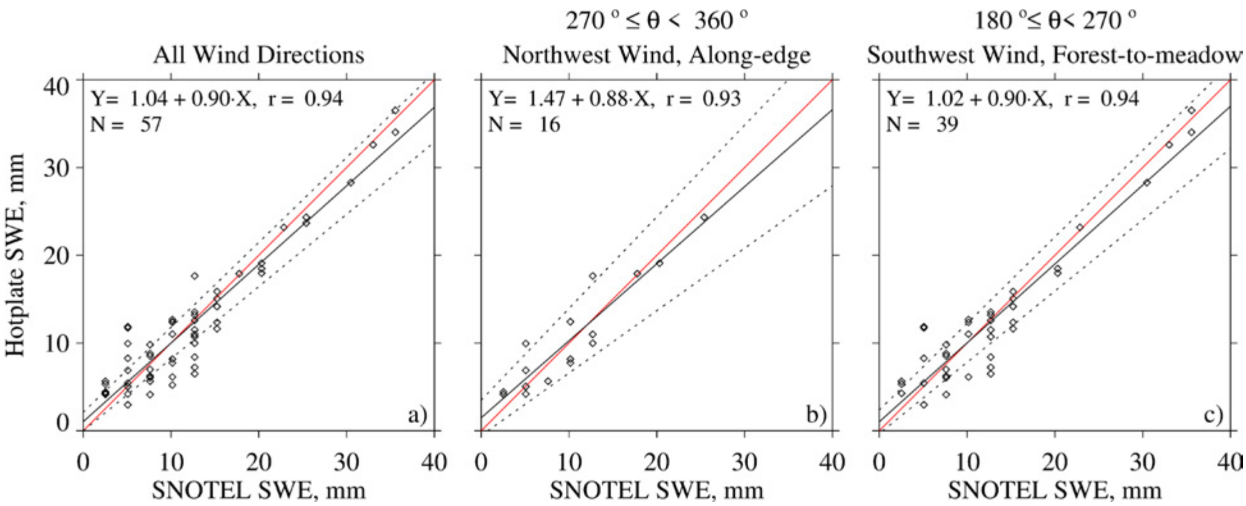

FIG. 9. (a) Group-1 analysis intervals. (b) Group-1 intervals with interval-averaged wind direction $270° \leq \theta < 360°$ (along the forest–meadow edge). (c) Group-1 intervals with interval-averaged wind direction $180° \leq \theta < 270°$ (from forest to meadow). In all panels, the regression line is the solid black line, the upper- and lower-limit regression threshold lines are the dashed lines, and one-to-one agreement is indicated by the red line.

southeast wind-direction groupings had zero and two analysis intervals, respectively, and are not discussed further.

b. NADP NOAH-IV versus NCAR (group 2)

Figure 10a is a scatterplot of the group-2 analysis intervals with sample size $N = 130$. The wind-exposed gauge measurements (NADP NOAH-IV) are on the y axis and the sheltered gauge measurements (NCAR) are on the x axis. Figures 10b–d show the comparisons for three of the 30° wind sectors illustrated in Fig. 7. There was one analysis interval that classified with wind direction between 310° and 340° and that is not discussed further. There were no analysis intervals with wind directions from 340° to 360° or from 0° to 220°.

Because easterly wind (direction between 0° and 180°) precluded targeting of the ice nucleating aerosol investigated by Breed et al. (2014), such analysis intervals are not a subset of the group-2 intervals (section 3c). Although their frequency of occurrence is less, snowfall associated with easterly flow does occur within the Medicine Bow Mountains. These are characterized by airflow that is meadow-to-forest within the study area. This contrasts with the forest-to-meadow air flows considered here. The meadow-to-forest/easterly events would provide a counterpoint to this analysis, and they should be examined in future research.

c. Wind direction

Several group-1 analysis intervals include frontal passages with southwesterly winds prior to the front and northwesterly winds after frontal passage; other group-1 intervals exhibit steady westerly winds. Nearly all the group-2 intervals have wind directions between southwesterly and northwesterly. These group-1 and group-2 characteristics are evident in the graphed AmeriFlux sequences referenced in the data availability statement.

Two null hypotheses, both with relevance to the snow-fence hypothesis of section 3b, were evaluated: 1) The regression equation y axis intercepts in Figs. 9 and 10 are indistinguishable from zero ($a = 0$), and 2) the regression equation slopes in Figs. 9 and 10 are indistinguishable from one ($b = 1$). The sixth and ninth columns of Table 3 contain the probabilities that the null hypotheses are true. Also in Table 3 are the values of a, σ_a, b, and σ_b (section 3e) applied in the hypothesis testing.

The along-edge group-1 subset (Fig. 9b) has regression threshold lines (section 3e) that encompass one-to-one and has p values for intercept and slope that are greater than the critical value (0.05; section 3e). These results provide support for the null hypotheses that $a = 0$ and $b = 1$. The results therefore indicate the absence of a snow-fence effect. The forest-to-meadow subset (Fig. 9c) also has regression threshold lines that encompass one-to-one and a p value for intercept >0.05. These characteristics also provide support for the absence of a snow-fence effect. However, the p value for slope is marginally smaller than 0.05 and thus the alternate hypothesis should be accepted. This inference is driven by a majority of the largest seven X/Y data pairs deviating below the one-to-one line. It is noted that these deviations are opposite the expectation for a snow-fence effect. On balance, it seems fair to conclude that there is not strong evidence for a snow-fence effect in group 1.

As was discussed, several of the group-1 analysis intervals (13 of 57) have frontal passages and associated wind shifts. The 24-h wind averaging, at least for these 13 intervals, may make the averaged wind data (directions and speeds) unrepresentative of processes contributing to a snow-fence effect. To address this, we redid the group-1 processing by dividing each of the 24-h analysis intervals into six four-hour averaging intervals. Two changes resulted from four-hour vs 24-h averaging: 1) Regression line intercepts changed sign from 1.47 to -0.76 mm (along-edge subset) and from 1.02 to -0.68 mm

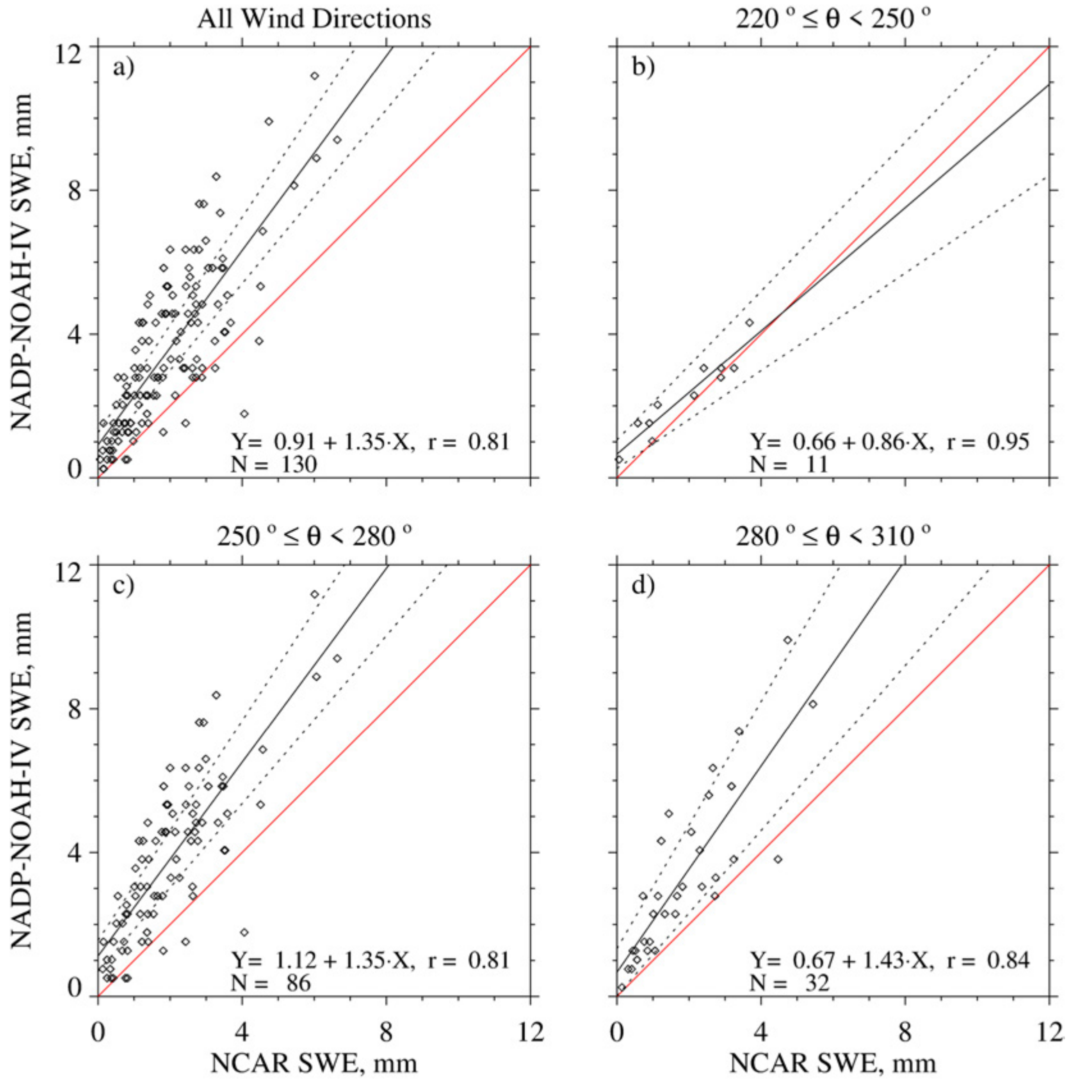

FIG. 10. (a) Group-2 analysis intervals. (b) Group-2 intervals with interval-averaged wind direction $220° \leq \theta < 250°$. (c) Group-2 intervals with interval-averaged wind direction $250° \leq \theta < 280°$. (d) Group-2 intervals with interval-averaged wind direction $280° \leq \theta < 310°$. In all panels, the regression line is the solid black line, the upper- and lower-limit regression threshold lines are the dashed lines, and one-to-one agreement is indicated by the red line.

(meadow-to-forest subset), and 2) the regression line slopes, both for the along-edge subset and for the forest-to-meadow subset, did not depart significantly from one. These changes are also not consistent with a snow-fence effect.

Figure 7 shows group-2 landscape characteristics for the wind sectors discussed in section 4b. The relevant scatterplots are Figs. 10b–d. Of these, the $220° \leq \theta < 250°$ sector is different from the other two ($250° \leq \theta < 280°$ and $280° \leq \theta < 310°$) with larger edge-to-gauge distance, fewer trees immediately upwind of the gauge, and a smaller exposed-vs-sheltered SWE slope ($b = 0.86$, Fig. 10b). Despite the fewer number of points in this wind sector, the better agreement between NADP NOAH-IV and NCAR, especially at larger values of SWE where there is greater confidence in the measurements, could be indicating a weaker source for wind-remobilized snow particles, in comparison with the other two sectors. In the latter, slopes are substantially greater than 1, the slope t tests indicate support for the alternate hypothesis, and the intercept t tests indicate strong or marginal support for the alternate hypothesis (Table 3). Based on these findings, it is concluded that there is support for a snow-fence effect in group 2.

d. Wind speed

Interval-averaged wind speeds (section 3d) were correlated with a quantity that was derived using SWE measurements from the paired (wind-exposed and sheltered) precipitation gauge systems. The derived quantity is the orthogonal displacement of an exposed/sheltered SWE pair from one-to-one. Section 3c explains that these displacements were

TABLE 3. Testing of regression statistics presented in Figs. 9 and 10, with wind directions, Df values, intercepts, intercept uncertainties, intercept p values, slopes, slope uncertainties, and slope p values.

Figure	Wind direction	Df	a (mm)	σ_a (mm)	p value for a (intercept t test)	b	σ_b	p value for b (slope t test)
9a	All	55	1.04	0.64	0.06	0.90	0.04	0.01
9b	Northwest (along edge)	14	1.47	1.14	0.11	0.88	0.09	0.11
9c	Southwest (forest to meadow)	37	1.02	0.80	0.10	0.90	0.05	0.03
10a	All	128	0.91	0.21	<0.01	1.35	0.09	<0.01
10b	$220° \le \theta < 250°$	9	0.66	0.22	0.01	0.86	0.10	0.09
10c	$250° \le \theta < 280°$	84	1.12	0.26	<0.01	1.35	0.11	<0.01
10d	$280° \le \theta < 310°$	30	0.67	0.39	0.05	1.43	0.17	0.01

assigned > 0 for exposed SWE > sheltered SWE and assigned < 0 for exposed SWE < sheltered SWE.

For group 1, there is not a significant correlation ($r = 0.00$; $N = 57$) between orthogonal displacement and wind speed (Fig. 11a). That result is based on 24-h wind averaging (section 4c). The absence of a significant correlation is also true in the case of four-hour wind averaging ($r = -0.07$; $N = 213$) (not shown). Both results are counter to the snow-fence hypothesis of section 3b, that is, our statement that an exposed gauge registers more snow deposition than does a sheltered gauge (orthogonal displacement > 0) and that this enhancement increases with wind speed. However, in Fig. 11b, there is a positive correlation between orthogonal displacement and wind speed ($r = 0.44$; $N = 130$). The authors surmise this is because of a snow-fence effect operating at the exposed group-2 gauge (NADP NOAH-IV). It is important to note that none of the group-2 measurements were post hoc corrected for undercatch. However, because wind speed was likely larger at the exposed group-2 site (NADP) than at the sheltered group-2 site (NCAR), where wind speed was seldom larger than 2 m s^{-1} (Breed et al. 2014), it seems reasonable to assert that the true magnitude of the wind-induced snow deposition enhancement was larger than evident in either Figs. 11b or 10a.

e. NADP NOAH-IV measurement quality assurance

The NADP NOAH-IV measurements were examined for bias by comparing them to measurements from the Belfort gauge. The latter was also operated at the NADP site and was also Alter shielded (section 2d). The basis for the comparison is 24-h precipitation amounts (rain and snow) with the condition that both gauges reported > 1 mm. Data from both gauges are available from 2011 to 2014. Figures 12a and 12b show the comparisons for June–August (JJA; Fig. 12a) and December–February (DJF; Fig. 12b). The JJA group is rain or hail ($T > +5°C$) and the DJF group is snow ($T < -2°C$).

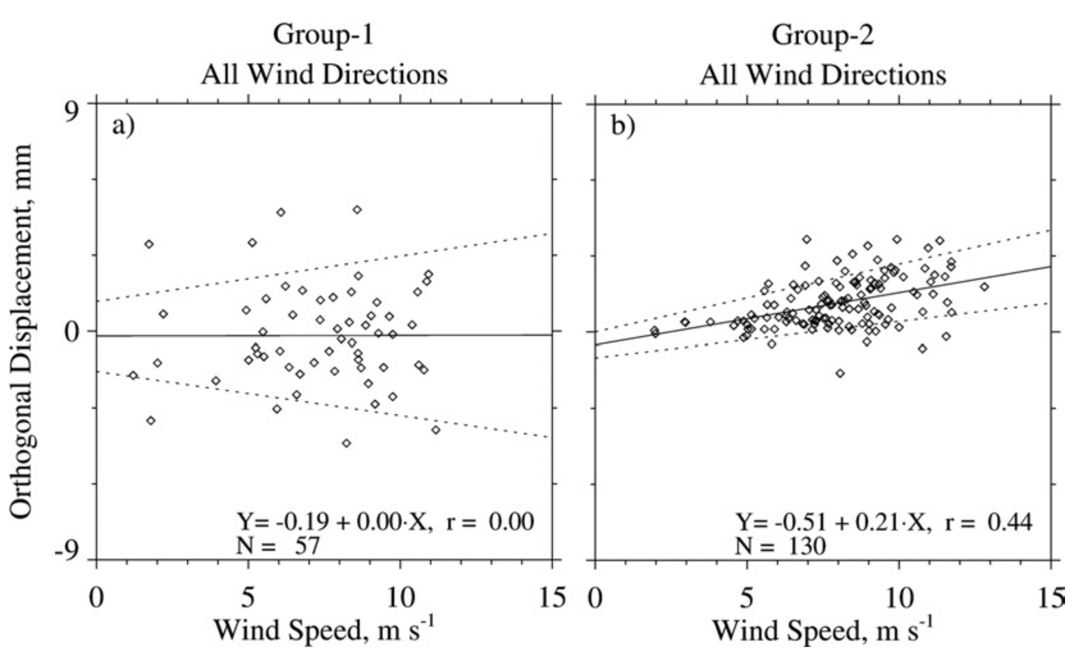

FIG. 11. (a) Group-1 orthogonal displacement vs group-1 interval-averaged wind speed. (b) Group-2 orthogonal displacement vs group-2 interval-averaged wind speed. In both panels, the regression line is the solid black line and the upper- and lower-limit regression threshold lines are the dashed lines.

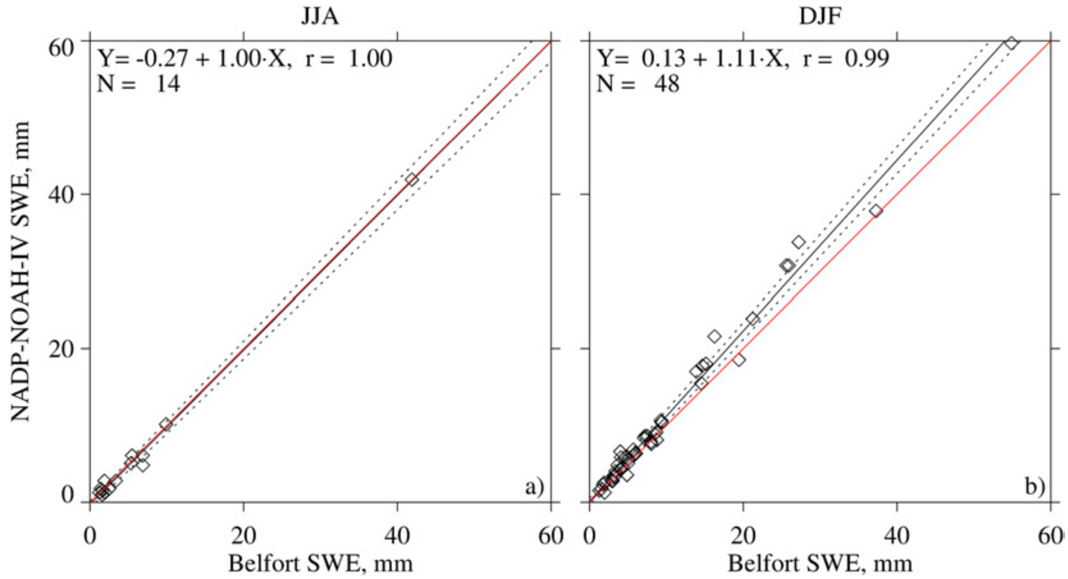

FIG. 12. (a) JJA precipitation measurements from the NADP NOAH-IV and Belfort gauges. (b) DJF precipitation measurements from the NADP NOAH-IV and Belfort gauges. In (a) and (b), the regression line is the solid black line, the upper- and lower-limit regression threshold lines are the dashed lines, and one-to-one agreement is indicated by the red line.

Some of the NADP NOAH-IV/Belfort data pairs available for the comparison were discarded because they had fewer than 288 Belfort samples. This discarding is consistent with the Belfort sampling interval (Table 2) and the duration of the comparisons (24 h). However, because a sample container weight acquired at the beginning and at the end of a comparison interval are sufficient for evaluating a Belfort precipitation amount, the discarding may be too restrictive. When compared with Figs. 12a and 12b, revised figures that include comparison intervals with fewer than 288 Belfort samples have ~30% more points and larger variance (results not shown). The discarding does not change the following: 1) Fig. 12a suggests reasonable agreement for rain and hail (JJA), and 2) Fig. 12b suggests that in snow (DJF) either the NADP NOAH-IV was high biased by 11%, or the Belfort was low biased by 11%. The high bias was accounted for by decreasing the NADP NOAH-IV values by 11% in a revised Fig. 10 (not shown). The revised figure shows, as in Fig. 10, that three of the four regression lines plot significantly above the one-to-one line (as in Figs. 10a,c,d) and that at SWE > 2 mm the two regression threshold lines encompass the one-to-one line (as in Fig. 10b).

f. NCAR measurement quality assurance

In section 2e, it was assumed that wind speeds at the sheltered NCAR site were small enough to forgo an undercatch correction. This was tested by comparing the group-2 NCAR values to pillow measurements acquired at the SNOTEL site. The null hypothesis is that the average of NCAR − SNOTEL is < 0 mm. The latter would indicate that the NCAR values were negatively biased, relative to the SNOTEL, and perhaps because the NCAR values were not corrected for undercatch. The average of NCAR–SNOTEL is 0.2 mm, and the standard deviation is 3.2 mm ($N = 129$, as compared with Fig. 10, where $N = 130$; one comparison interval was rejected because SNOTEL data were unavailable). Using a t-distribution calculator (section 3e), the null hypothesis was not rejected (Df = 128, $t = 0.89$, and $p = 0.19$). However, the null hypothesis was rejected after the three most outlying data pairs—all with an absolute difference between NCAR and SNOTEL larger than 6 mm—were discarded (Df = 125, $t = 3.0$, and $p < 0.01$). This supports the assertion that the NCAR gauge measurements do not require an undercatch correction. It also implies that the problem of correcting the NCAR gauge measurements with height-extrapolated AmeriFlux tower wind measurements can be avoided.

g. Exposed-to-sheltered SWE ratios

Figure 10 demonstrates that the wind-exposed group-2 SWE measurements generally exceeded the sheltered group-2 SWE measurements, and more so for particular wind-direction sectors. Underlying this dependence on wind direction is a dependence on wind speed. This wind speed dependence was investigated by calculating three exposed-to-sheltered SWE ratios. In Williams et al. (1998) this ratio is 1.6. The exposed-to-sheltered SWE ratios in this analysis were derived in two steps. First, the NADP NOAH-IV and NCAR SWE values were separately summed within each of the wind-direction groups of Figs. 10b–d. Second, the exposed-to-sheltered ratios were formulated as the NADP NOAH-IV summation divided by the NCAR summation. Consistent with Fig. 10, the exposed-to-sheltered ratio is smaller (1.2) for the $220° \le \theta < 250°$ sector, and larger for the $250° \le \theta < 280°$ and $280° \le \theta < 310°$ sectors (1.9 and 1.8, respectively). Mean wind speeds for these sectors are 6.5, 8.3, and 7.8 m s^{-1}, respectively. These exposed-to-sheltered ratios, and the associated wind speeds, indicate that larger wind speed is a factor leading to more snow deposition at the wind-exposed NADP site than at the sheltered NCAR site. This result is consistent with the snow-fence hypothesis of section 3b.

5. Conclusions

Analyzed herein are snow deposition and wind measurements acquired using ground- and tower-based measurement systems. Observations were taken at multiple sites east of the crest of the Medicine Bow Mountains in southeastern Wyoming. Two groups of measurements were analyzed. A comparison was performed within each group to evaluate snow deposition differences as they relate to wind speed, wind direction, and forest coverage.

The group-1 analysis demonstrated that there is reasonable agreement between the Hotplate and SNOTEL SWE values. A modified R11 Hotplate catch efficiency was applied in this comparison. It was concluded that a snow-fence effect is not evident in the group-1 data. The group-2 analysis demonstrated that larger SWE values occurred at the wind-exposed NADP site relative to the sheltered NCAR site; it also demonstrated that this disagreement increased with wind speed. Additionally, wind sectors with greater upwind forest coverage and a shorter tree-to-gauge distance were shown to exhibit greater disagreement. It was concluded that a snow-fence effect is evident in the group-2 data. Supporting this is photography of locally enhanced snow deposition in the Medicine Bow Mountains of southeast Wyoming (Hiemstra et al. 2006, their Fig. 3) and a comparison with wind-exposed and sheltered gauge measurements made above tree line in the northern Colorado Rocky Mountains (Williams et al. 1998).

Overall, this work indicates that a snow-fence effect can enhance snow deposition at an exposed NADP monitoring site and that the maximum extent of this enhancement is approximately a factor of 2. It is recommended that future investigators analyze the meadow-to-forest/easterly events not examined here, that models capable of quantifying wind-driven snow particle resuspension and deposition be improved, and that planning done for a proposed monitoring site or for changing an existing monitoring site acknowledge how snow deposition, and the deposition of chemical constituents carried by snow, can be altered by the snow-fence effect.

Acknowledgments. We thank the National Science Foundation (Award 1850809) and the John P. Ellbogen Foundation for funding. We also thank Chad Hutchens for preparing the digital object identifiers.

Data availability statement. Gauge measurements from the NCAR site were obtained from K. Ikeda (2017, personal communication). NADP NOAH-IV gauge measurements were obtained from J. Korfmacher (2017, personal communication). Belfort gauge measurements were obtained from J. Frank (2021, personal communication). Hotplate gauge measurements (https://doi.org/10.15786/20103146), Brooklyn Lake SNOTEL measurements (https://wcc.sc.egov.usda.gov/nwcc/site?sitenum=367), and U.S.-GLE AmeriFlux measurements (https://ameriflux.lbl.gov/) are available online. Merged, tabulated, and graphed Hotplate, SNOTEL, NCAR, NADP NOAH-IV, and AmeriFlux datasets are available online (https://doi.org/10.15786/20247870).

REFERENCES

Alter, J. C., 1937: Shielded storage precipitation gauges. *Mon. Wea. Rev.*, **65**, 262–265, https://doi.org/10.1175/1520-0493(1937)65<262:SSPG>2.0.CO;2.

AmeriFlux, 2021: U.S.-GLE data. Accessed 10 December 2019, https://ameriflux.lbl.gov/sites/siteinfo/US-GLE.

Borkhuu, B., 2009: Snowfall at a high-elevation site: Comparisons of six measurement techniques. M.S. thesis, Dept. of Atmospheric Science, University of Wyoming, 143 pp.

Breed, D., R. Rasmussen, C. Weeks, B. Boe, and T. Deshler, 2014: Evaluating winter orographic cloud seeding: Design of the Wyoming Weather Modification Pilot Project (WWMPP). *J. Appl. Meteor. Climatol.*, **53**, 282–299, https://doi.org/10.1175/JAMC-D-13-0128.1.

Burns, D. A., 2003: Atmospheric nitrogen deposition in the Rocky Mountains of Colorado and southern Wyoming—A review and new analysis of past study results. *Atmos. Environ.*, **37**, 921–932, https://doi.org/10.1016/S1352-2310(02)00993-7.

Cassiani, M., G. G. Katul, and J. D. Albertson, 2008: The effects of canopy leaf area index on airflow across forest edges: Large-eddy simulation and analytical results. *Bound.-Layer Meteor.*, **126**, 433–460, https://doi.org/10.1007/s10546-007-9242-1.

Cauteruccio, A., M. Colli, M. Stagnaro, L. G. Lanza, and E. Vuerich, 2021: In-situ precipitation measurements. *Springer Handbook of Atmospheric Measurements*, T. Foken, Ed., Springer Handbooks, Springer, 359–400, https://doi.org/10.1007/978-3-030-52171-4_12.

Chen, M., P. Xie, J. E. Janowiak, and P. A. Arkin, 2002: Global land precipitation: A 50-yr monthly analysis based on gauge observations. *J. Hydrometeor.*, **3**, 249–266, https://doi.org/10.1175/1525-7541(2002)003<0249:GLPAYM>2.0.CO;2.

Colorado Avalanche Information Center, 2022: Weather stations. Accessed 1 July 2022, https://lb.avalanche.state.co.us/weather-stations-measuring-precipitation/.

ETI Instrument Systems, 2020: NOAH IV total precipitation gauge configured for the National Atmospheric Deposition Program. Tech. Manual, 24 pp., https://nadp.slh.wisc.edu/wp-content/uploads/2021/09/ETI_NOAHIV_Manual.pdf.

Fujiyoshi, Y., T. Endoh, T. Yamada, K. Tsuboki, Y. Tachibana, and G. Wakahama, 1990: Determination of a *Z*–*R* relationship for snowfall using a radar and high sensitivity snow gauges. *J. Appl. Meteor.*, **29**, 147–152, https://doi.org/10.1175/1520-0450(1990)029<0147:DOARFS>2.0.CO;2.

Fuller, S., S. A. Marlow, S. Haimov, M. Burkhart, K. Shaffer, A. Morgan, and J. R. Snider, 2023: W-band *S*–*Z* relationships for rimed snow particles: Observational evidence from combined airborne and ground-based observations. *Atmos. Meas. Tech.*, **16**, 6123–6142, https://doi.org/10.5194/amt-16-6123-2023.

Goodison, B. E., 1978: Accuracy of Canadian snow gage measurements. *J. Appl. Meteor.*, **17**, 1542–1548, https://doi.org/10.1175/1520-0450(1978)017<1542:AOCSGM>2.0.CO;2.

——, P. Louie, and D. Yang, 1998: WMO solid precipitation measurement intercomparison. Instruments and Observing Methods Rep. 67, WMO/TD-872, 318 pp., https://library.wmo.int/viewer/28336.

Groisman, P. Ya., and D. R. Legates, 1994: The accuracy of United States precipitation data. *Bull. Amer. Meteor. Soc.*, **75**, 215–228, https://doi.org/10.1175/1520-0477(1994)075<0215:TAOUSP>2.0.CO;2.

——, and Coauthors, 1999: Changes in the probability of heavy precipitation: Important indicators of climatic change. *Weather and Climate Extremes*, Springer, 243–283.

Gultepe, I., A. J. Heymsfield, P. R. Field, and D. Axisa, 2017: Ice-phase precipitation. *Ice Formation and Evolution in Clouds and Precipitation: Measurement and Modelling Challenges*, *Meteor. Monogr.*, No. 58, Amer. Meteor. Soc., https://doi.org/10.1175/AMSMONOGRAPHS-D-16-0013.1.

Harrison, D. L., S. J. Driscoll, and M. Kitchen, 2000: Improving precipitation estimates from weather radar using quality control and correction techniques. *Meteor. Appl.*, **7**, 135–144, https://doi.org/10.1017/S1350482700001468.

Hiemstra, C. A., G. E. Liston, and W. A. Reiners, 2006: Observing, modelling, and validating snow redistribution by wind in a Wyoming upper treeline landscape. *Ecol. Modell.*, **197**, 35–51, https://doi.org/10.1016/j.ecolmodel.2006.03.005.

Kennedy, A., A. Scott, N. Loeb, A. Sczepanski, K. Lucke, J. Marquis, and S. Waugh, 2022: Bringing microphysics to the masses: The Blowing Snow Observations at the University of North Dakota: Education through Research (BLOWN-UNDER) campaign. *Bull. Amer. Meteor. Soc.*, **103**, E83–E100, https://doi.org/10.1175/BAMS-D-20-0199.1.

Kitzmiller, D., D. Miller, R. Fulton, and F. Ding, 2013: Radar and multisensor precipitation estimation techniques in National Weather Service hydrologic operations. *J. Hydrol. Eng.*, **18**, 133–142, https://doi.org/10.1061/(ASCE)HE.1943-5584.0000523.

Kochendorfer, J., and Coauthors, 2018: Testing and development of transfer functions for weighing precipitation gauges in WMO-SPICE. *Hydrol. Earth Syst. Sci.*, **22**, 1437–1452, https://doi.org/10.5194/hess-22-1437-2018.

Lehmann, C. M. B., V. C. Bowersox, and S. M. Larson, 2005: Spatial and temporal trends of precipitation chemistry in the United States, 1985–2002. *Environ. Pollut.*, **135**, 347–361, https://doi.org/10.1016/j.envpol.2004.11.016.

Li, Y., and Coauthors, 2016: Increasing importance of deposition of reduced nitrogen in the United States. *Proc. Natl. Acad. Sci. USA*, **113**, 5874–5879, https://doi.org/10.1073/pnas.1525736113.

Martinaitis, S. M., S. B. Cocks, Y. Qi, B. T. Kaney, J. Zhang, and K. Howard, 2015: Understanding winter precipitation impacts on automated gauge observations within a real-time system. *J. Hydrometeor.*, **16**, 2345–2363, https://doi.org/10.1175/JHM-D-15-0020.1.

Matrosov, S. Y., 2007: Modeling backscatter properties of snowfall at millimeter wavelengths. *J. Atmos. Sci.*, **64**, 1727–1736, https://doi.org/10.1175/JAS3904.1.

Metcalfe, J. R., and B. E. Goodison, 1992: Automation of winter precipitation estimates: The Canadian experience. Instruments and Observing Methods Rep. 49, WMO/TD-462, 81–85.

Meyer, J. D. D., J. Jin, and S. Wang, 2012: Systematic patterns of the inconsistency between snow water equivalent and accumulated precipitation as reported by the snowpack telemetry network. *J. Hydrometeor.*, **13**, 1970–1976, https://doi.org/10.1175/JHM-D-12-066.1.

NADP, 2021: National Atmospheric Deposition Program. http://nadp.slh.wisc.edu/.

Nanus, L., J. A. McMurray, D. W. Clow, J. E. Saros, T. Blett, and J. J. Gurdak, 2017: Spatial variation of atmospheric nitrogen deposition and critical loads for aquatic ecosystems in the greater Yellowstone area. *Environ. Pollut.*, **223**, 644–656, https://doi.org/10.1016/j.envpol.2017.01.077.

Nellis, G. F., and S. A. Klein, 2021: *Introduction to Engineering Heat Transfer*. Cambridge University Press, 1001 pp.

Nešpor, V., and B. Servuk, 1999: Estimation of wind-induced error of rainfall gauge measurements using a numerical simulation. *J. Atmos. Oceanic Technol.*, **16**, 450–464, https://doi.org/10.1175/1520-0426(1999)016<0450:EOWIEO>2.0.CO;2.

Nitu, R., and K. Wong, 2010: CIMO survey on national summaries of methods and instruments for solid precipitation measurement at automatic weather stations. Instruments and Observing Methods Rep. 102, WMO/TD-1544, 57 pp., https://library.wmo.int/viewer/50474.

NRCS, 2021: Brooklyn Lake SNOTEL. Accessed 10 December 2019, https://wcc.sc.egov.usda.gov/nwcc/site?sitenum=367.

Panofsky, H. A., and J. A. Dutton, 1984: *Atmospheric Turbulence*. Wiley-Interscience, 397 pp.

Pokharel, B., and G. Vali, 2011: Evaluation of collocated measurements of radar reflectivity and particle sizes in ice clouds. *J. Appl. Meteor. Climatol.*, **50**, 2104–2119, https://doi.org/10.1175/JAMC-D-10-05010.1.

Rasmussen, R., and Coauthors, 2012: How well are we measuring snow: The NOAA/FAA/NCAR winter precipitation test bed. *Bull. Amer. Meteor. Soc.*, **93**, 811–829, https://doi.org/10.1175/BAMS-D-11-00052.1.

——, J. Hallett, R. Purcell, S. D. Landolt, and J. Cole, 2011: The Hotplate precipitation gauge. *J. Atmos. Oceanic Technol.*, **28**, 148–164, https://doi.org/10.1175/2010JTECHA1375.1.

——, and Coauthors, 2018: Evaluation of the Wyoming Weather Modification Pilot Project (WWMPP) using two approaches: Traditional statistics and ensemble modeling. *J. Appl. Meteor. Climatol.*, **57**, 2639–2660, https://doi.org/10.1175/JAMC-D-17-0335.1.

Rinehart, R. E., 1983: Out-of-level instruments: Errors in hydrometeor spectra and precipitation measurements. *J. Climate Appl. Meteor.*, **22**, 1404–1410, https://doi.org/10.1175/1520-0450(1983)022<1404:OOLIEI>2.0.CO;2.

Rodell, M., and Coauthors, 2004: The Global Land Data Assimilation System. *Bull. Amer. Meteor. Soc.*, **85**, 381–394, https://doi.org/10.1175/BAMS-85-3-381.

Savina, M., B. Schäppi, P. Molnar, P. Burlando, and B. Sevruk, 2012: Comparison of a tipping-bucket and electronic weighing precipitation gauge for snowfall. *Atmos. Res.*, **103**, 45–51, https://doi.org/10.1016/j.atmosres.2011.06.010.

Serreze, M. C., M. P. Clark, R. L. Armstrong, D. A. McGinnis, and R. S. Pulwarty, 1999: Characteristics of the western United States snowpack from snowpack telemetry (SNOTEL) data. *Water Resour. Res.*, **35**, 2145–2160, https://doi.org/10.1029/1999WR900090.

Sieck, L. C., S. J. Burges, and M. Steiner, 2007: Challenges in obtaining reliable measurements of point rainfall. *Water Resour. Res.*, **43**, W01420, https://doi.org/10.1029/2005WR004519.

Skofronick-Jackson, G., and Coauthors, 2017: The Global Precipitation Measurement (GPM) mission for science and society. *Bull. Amer. Meteor. Soc.*, **98**, 1679–1695, https://doi.org/10.1175/BAMS-D-15-00306.1.

Thériault, J. M., R. Rasmussen, K. Ikeda, and S. Landolt, 2012: Dependence of snow gauge collection efficiency on snowflake characteristics. *J. Appl. Meteor. Climatol.*, **51**, 745–762, https://doi.org/10.1175/JAMC-D-11-0116.1.

Thompson, G., and T. Eidhammer, 2014: A study of aerosol impacts on clouds and precipitation development in a large winter cyclone. *J. Atmos. Sci.*, **71**, 3636–3658, https://doi.org/10.1175/JAS-D-13-0305.1.

Williams, M. W., T. Bardsley, and M. Rikkers, 1998: Overestimation of snow depth and inorganic nitrogen wetfall using NADP data, Niwot Ridge, Colorado. *Atmos. Environ.*, **32**, 3827–3833, https://doi.org/10.1016/S1352-2310(98)00009-0.

Wilson, J. W., and E. A. Brandes, 1979: Radar measurement of rainfall—A summary. *Bull. Amer. Meteor. Soc.*, **60**, 1048–1060, https://doi.org/10.1175/1520-0477(1979)060<1048:RMORS>2.0.CO;2.

Wolfe, J. P., and J. R. Snider, 2012: A relationship between reflectivity and snow rate for a high-altitude S-band radar. *J. Appl. Meteor. Climatol.*, **51**, 1111–1128, https://doi.org/10.1175/JAMC-D-11-0112.1.

Young, H. D., 1962: *Statistical Treatment of Experimental Data*. McGraw-Hill, 172 pp.

Zelasko, N., A. Wettlaufer, B. Borkhuu, M. Burkhart, L. S. Campbell, W. J. Steenburgh, and J. R. Snider, 2018: Hotplate precipitation gauge calibrations and field measurements. *Atmos. Meas. Tech.*, **11**, 441–458, https://doi.org/10.5194/amt-11-441-2018.